Where does the optically detectable aerosol in the European Arctic come from?

By Maria Stock[1]⋆, Christoph Ritter[1], Veijo Aaltonen[3], Wenche Aas[4], Dörthe Handorff[1], Andreas Herber[2], Renate Treffeisen[2] and Klaus Dethloff[1],

[1] *Alfred-Wegener-Institute for Polar and Marine Research in the Helmholtz Association, Telegrafenberg A 43, 14473 Potsdam, Germany*
[2] *Alfred-Wegener-Institute for Polar and Marine Research in the Helmholtz Association, Bürgermeister-Schmidt-Straße 20, 27568 Bremerhaven, Germany*
[3] *Climate and Global Change Research, Finnish Meteorological Institute, P.O. Box 503, 00101 Helsinki, Finland*
[4] *Norwegian Institute for Air Research, P.O. Box 100, 2027 Kjeller, Norway*

()

ABSTRACT

In this paper we pose the question where the source regions of the aerosol which occurs in the European Arctic are located. Long-term aerosol optical depth (AOD) data from Ny-Ålesund and Sodankylä as well as short data from a campaign on a Russian drifting station were analysed by air backtrajectories, analysis of the general circulation pattern and a correlation to chemical composition from in-situ measurements. Surprisingly our data clearly shows that direct transport of pollutants from Europe does not play an important role. Instead, Arctic haze in Ny-Ålesund has been found for air masses from the Eastern Arctic, while events with increased AOD but chemically more diverse composition have been found for air from Siberia or the central Arctic. Moreover, the AOD in Ny-Ålesund does not depend on the North Atlantic Oszillation (NAO). Hence, either the pollution pathways of aerosol are more complex or aerosol is significantly altered by clouds.

1 Introduction

The Arctic is climatologically a very sensitive region, where temperature increase was larger during the 20th century than compared to mid-latitudes ("Arctic amplification"). This holds true especially for springtime (Solomon et al., 2007), as an earlier onset of the melting season increases the snow-albedo feedback (Hall and Qu, 2006). During last years a strong decrease in Arctic sea ice was noticed. The September cover seems to retreat by -12.4 % per decade (Stroeve et al., 2012) which further enhances the near surface temperature (Screen and Simmonds, 2010). Such a retreat in sea ice has a potential impact on large scale circulation by supporting negative phases of the North Atlantic Circulation (NAO) as shown recently e.g. in Jaiser et al. (2012).

Aerosols influence the Arctic radiation budget in many ways. Directly they can scatter and absorb sunlight ("dimming") or, by deposition on the ground, lead to a decrease in albedo ("darkening"). Estimation of the net aerosol forcing is extremely difficult in the Arctic, as next to the sparseness of observational data also the strongly varying light conditions and the albedo in the run of the year have to be considered. Currently Stone et al. (2013) concluded that aerosol should contribute to a significant net surface cooling during the annual cycle. Of course the spatial distribution of aerosol is needed to assess the radiative effect. On the other hand our knowledge of precise microphysical properties of Arctic aerosols (size distribution, shape, index of refraction) is still limited. While the phenomenon of Arctic Haze for accumulation mode particles mainly consisting of sulphates and soot is known for many years (Shaw, 1995; Quinn et al., 2007), recently also biomass burning was found to be one of the important sourses of Arctic air pollution (Warneke et al., 2009; Stock et al., 2011) even in early spring.

Numerous studies are already related to the pollution pathways into the Arctic. The concept of the Polar-dome (or Arctic-dome) was introduced by Carlson (1981) and Iversen (1984) when trajectories of constant potential temperature form closed dome-like loops around the North pole. Air flows generally follow trajectories of constant potential temperatures, except for winter when diabatic cooling of air over cold surfaces occurs. Hence, already Shaw (1983) gave long range transport from Eurasia as main source for Arctic Haze and this picture was extended and refined all over the years (Stohl, 2006). Eckhardt et al. (2003) showed, using FLEXPART dispersion model (Stohl et al., 1998) and ECMWF re-analysis data (Gibson et al., 1999) that transport into the Arctic is facilitated at positive NAO phase. Especially tracers from Europe penetrate into the Arctic within 8-10 days at positive NAO phase. Eneroth et al. (2003) also used ECMWF data and clustered air backtrajectories arriving at Ny-Ålesund, Svalbard and found higher carbon dioxide val-

⋆ Corresponding author.
e-mail: christoph.ritter@awi.de

ues for air from Europe. Similarly, Fisher et al. (2010) were able to connect air with increased carbon monoxide concentration to backtrajectories from polluted sites in Europe and Asia from aircraft measurements. Rozwadowska et al. (2010) performed a cluster analysis of air backtrajectories over Spitsbergen and found indeed higher AOD for air from Eurasia.

From these studies one might think that air flow into the Arctic is reasonably well understood and that aerosols might directly follow the air trajectories. However, already Stock et al. (2011) reported higher AOD values over the more remote Russian drifting station NP-35 than over Ny-Ålesund. Moreover, Toledano et al. (2012) gave an overview of sun photometer measurements at different Arctic sites. They found that the typical springtime aerosol load expressed in monthly means of AOD was larger at sites on Svalbard than on mainland Scandinavia. Hence from their data it can already be assumed that the Arctic Haze phenomenon is only subtle over the European mainland. This poses already some doubts whether the above mentioned transport pathways can directly be applied to aerosol which is detectable by optical methods. For this reason we present in this work AOD time series and combined them to both, air backtrajectories and an EOF (empirical orthogonal functions) analysis of surface pressure. The scope of this work is to find out whether the omnipresent aerosol in the Arctic do follow the above mentioned "classical" transport routes.

Apparently there is no doubt that direct transport of polluted air from central Europe into the Arctic has been observed so far, see quotes here and in section 2.1. Also volcanic aerosol has been clearly identified in the Arctic (e.g. O'Neill (2012); Hoffmann et al. (2010)). For this reason few aerosol events that can be clearly assigned to a source have been omitted from this study. Nevertheless we will not only speak about background aerosol but also on hazy conditions with increased or even high AOD.

In this paper we present results from sun photometer measurements, mainly from Ny-Ålesund, but also from Sodankylä and the Russian drifting station NP-35 with observations from spring 2008 and compared the aerosol optical depth (AOD) with a cluster analysis of air backtrajectories (section 4), with an analysis of empirical orthogonal functions (EOF) of surface pressure (section 5) and correlate AOD to trace gas measurements (section 6). By this we want to demonstrate the difficulties to connect the measured Arctic AOD with unique source regions.

2   Instrumentation and Measurements

Three types of sun photometer (SP1A, SP2H, PFR) were operated at three locations (Ny-Ålesund, Sodankylä, NP-35, see Figure 1). They all differed in the number of employed interference filters (see Table 1). At least the SP1A and the PFR participated at an Arctic intercomparison experiment (Mazzola et al., 2012). For all data sets a cloud screening has been performed.

The aerosol optical depth τ is calculated based on the Lambert–Beer law:

$$I = I_0 \cdot e^{-m \cdot \tau_{ext}} \tag{1}$$

where I is the direct solar signal at the ground, I_0 the ex-

traterrestrial signal of the instrument and m the optical air mass. The equation (1) is modified based on the WMO recommendations (WMO, 1996) to retrieve τ at different wavelength λ:

$$\tau_A(\lambda) = \frac{\ln \frac{I_0(\lambda)}{K \cdot I(\lambda)} - m_R \cdot \tau_R(\lambda) - m_G \cdot \tau_G(\lambda)}{m_A} \tag{2}$$

The contributions of aerosol (A), absorbing gases (G) and molecules (R) were separated, also the Sun-Earth distance (K) is corrected. In general the estimated uncertainty of τ_{500nm} is 0.01–0.02 (Stock, 2010).

Besides τ_{500nm} the Ångström coefficient α is calculated from the regression line $\ln \tau_A(\lambda) = \ln \beta + (-\alpha) \cdot \ln \lambda$. For this regression were taken all available wavelengths not contaminated by any error signal.

2.1   Ny-Ålesund

The sun photometer measurements started in 1991 in the new established German research station AWIPEV (formerly "Koldewey") in Ny-Ålesund (78.9 °N, 11.9 °E, referred as Ny-Ålesund). Due to the eruption of the Pinatubo in the same year we only consider sun photometer measurements after 1995 here (Herber et al., 2002). Also we clear events of direct pollution from Europe, classical Arctic Haze from March 2000 (Yamanouchi et al., 2005) and March 2008 (Stock et al., 2011), two events of biomass burning - one event in July 2004 (Stohl et al., 2006), and second one in May 2006 (Stohl et al., 2007) - as well as one case of stratospheric aerosol caused by the Kasatochi volcano in August 2008 (Hoffmann et al., 2010). In total AOD data from 16 days out of total 412 days have been removed. We are aware that by omitting these events the influence of pollution from Europe and Siberia will be decreased, however we believe that this reduced data set is much more representative to the typical conditions in the Arctic. The remaining period 1995–2008 includes a total number of 65693 minutes of measurements. The used sun photometer types are SP2H and SP1A produced by Dr. Schulz und Partner GmbH, Germany.

2.2   Sodankylä

The facility of the Arctic Research Centre (67.37 °N, 26.65 °O, 190 m a.s.l.) in Sodankylä is part of Finnish Meteorological Institute Arctic Research Division. The research conducted there ranges from polar ozone and arctic snow coverage under the influence of global warming to the auroral observations. This boreal zone station is situated around 100 km north of polar circle and is surrounded by pine forest. Sun photometer measurements there have been conducted since summer 2004 with PFR (Precision Filter Radiometer, Physikalisch-Meteorologisches Observatorium Davos/World Radiation Center, Switzerland). The used data set encompasses measurements from 2004 till 2007 with a total number of 30904 1-min measurements.

2.3   NP-35

From September 2007 until April 2008 our colleague Jürgen Gräser participated at 35th North Pole drifting station (NP-35) and operated among others a sun photometer,

type SP1A. The sun photometer measurements were taken between the period 14 March and 7 April, 2008 and provided in total a number of 430 minutes of measurements. During that time NP 35 drifted from 56.7 °E to 42.0 °E and 85.5 °N to 84.2 °N (see Figure 1).

3   Methods

3.1   Trajectory calculation and cluster analysis

For the identification of aerosol source regions 5-day backward trajectories were calculated with PEP-Tracer (Pole-Equator-Pole Tracer, Orgis et al. (2009)). On the basis of the operational ECMWF three-dimensional wind fields ensembles of 1000 backward trajectories starting from an area of 25x25 km^2 around Ny-Ålesund, Sodankylä and NP-35 every six hours (00, 06, 12 and 18 UTC) were determined. As starting heights the standard pressure levels of 850, 700 and 500 hPa were chosen, assuming that they represent boundary layer, as well as lower free and upper troposphere. For each ensemble a mean trajectory was calculated and allocated to the measurements in the following way: for the start time X of each trajectory all measurements were allocated in the time range -3h < X < +2h.

We used only one total run time, which was 120 hours. Stock et al. (2011) have shown that sparse data in the Arctic hinders a trustful calculation beyond this period independent of the used meteorological data set. Typically, after 5 days the spread was about 300 km and 20 hPa horizontally and vertically for the 850 hPa trajectories and even larger for the higher ones (due to increasing wind speed with altitude). Hence, a clear classification would not have been possible with longer backtrajectories.

The clustering of the trajectories was performed using the non-hierarchical method k-means (MacQueen, 1967). In a first step k points (k- number of clusters) were randomly selected and used as reference center. Thereafter every k-point was allocated to the nearest point (distance minimization) and a new reference center were determined. This process was repeated until all points were allocated to a reference point. Because of the randomly selected start points, the process was run 20 times and the run with the lowest overall distance was chosen.

Trajectories of all heights were clustered in one step. This is necessary, because the measured AOD is a column value and it is not known at which height the aerosol was transported. Only if all heights of a start time were allocated to the same cluster, the measured AOD was assigned to this cluster. This approach guarantees a well-defined determination of the aerosol source region.

Before the cluster analysis can be applied, the number of clusters k has to be selected for each station separately. The minimum number of k was determined on the basis of total spatial variance (Stunder, 1996; Dorling et al., 1992). The maximum number of clusters can be derived by comparing the horizontal spread of the trajectories to the distances of the derived cluster centers. For our data set 8 clusters for Ny-Ålesund, 6 for Sodankylä and 4 for the NP-35 were optimal.

3.2   Empirical orthogonal function method

To see whether a connection between AOD and the large-scale circulation patterns exists, the empirical orthogonal function (EOF) analysis have been used (e.g., Preisendorfer, 1988; Hannachi et al., 2007). By applying EOF-analysis to a climate field it is possible to find the most important patterns explaining the variability of that field and to represent the data field compactly in terms of EOFs. By applying an EOF analysis the anomaly field $\vec{Z}'(j,t)$ of a climate field $\vec{Z}(j,t)$ is projected onto the space spanned by the EOFs:

$$\vec{Z}' = \sum_{j=1}^{J} \alpha'_j(t)\vec{e_j}. \tag{3}$$

Here $\vec{e_j}$, $(j = 1, ..., J)$ are the empirical orthogonal functions (EOF) which represents the spatial patterns. The time-dependent amplitude $\alpha'_j(t)$ of $\vec{e_j}$ is called the jth principal component (PC) of the time-series. The EOFs are the eigenvectors $\vec{e_j}$ of the covariance matrix of the field $\vec{Z}'$. The corresponding eigenvalues are proportional to the amount of variance explained by each eigenvector. Before calculating the covariance matrix, equal-area weighting is ensured by multiplying the fields with the square root of the cosine of latitude. All EOF patterns are re-normalised by the square root of the corresponding eigenvalues. Thus, the corresponding PC time-series $\alpha_j(t)$ are standardised (cf. von Storch and Zwiers, 2001).

By means of the EOF analysis, information about the spatial structure of the most dominant variability patterns (in terms of EOF-vectors) as well as about the temporal evolution of the teleconnection patterns (in terms of PC-time series) is obtained. Thus, the first EOF explains most of the variance of the data field.

To analyse the link between atmospheric circulation pattern and measured AOD over the Arctic, here we calculated the variability of the large-scale circulation in the lower to middle troposphere north of 50°N. Therefore, we applied the EOF-analysis to the fields of monthly and daily averages of the 6-hourly fields of mean sea-level pressure and geopotential height at 850, 700 and 500hPa for the winter season (DJF) and to the spring month March and April from 1995-2008 (daily means). All these data fields are provided from the ECMWF ERA-40 reanalysis ((Uppala et al., 2005)).

The physical interpretation of the atmospheric pattern found with the EOF has to be done carefully, because the EOF is a strictly mathematical analysis method (Dommenget and Latif, 2002) and must not necessarily represent physical quantities. However, later we will show that we find a pattern similar to the NAO as the most important EOF for the winter months.

4   Trajectory analysis

4.1   Ny-Ålesund

Due to the constrain that the trajectories of all 3 analysed heights had to belong to the same cluster, 322 (out of 1375) trajectories had been included in this study. The results of the clustering are shown in Figure 2 and Figure 3. In

Figure 2 the trajectory groups of all three heights are drawn in different colors. In Figure 3 the group means of τ_{500nm} and α, including their standard deviation, and the number of allocated hourly means are plotted. Three seasons were distinguished:

spring (red)	-	March, April, May,
summer (green)	-	June, July,
autumn (blue)	-	August, September.

It can be seen, that the highest τ_{500nm} values are generally observed in spring and decreasing values in the other months with the lowest τ_{500nm} in autumn. The same behavior is found for the standard deviation of τ_{500nm}, so obviously the spring atmosphere is more variable in advection efficiency. For trajectories coming from north (group 2 Beaufort Sea and group 1 East Arctic/Siberia) in spring the τ_{500nm} reaches maximum mean values of 0.13±0.03 and 0.11±0.03, respectively. This is followed by groups 6 and 4 (Central Arctic, Northeast Canada) with 0.1±0.04 and 0.1±0.02, respectively. Lowest τ_{500nm} in spring are observed in groups 5 and 8 (Europe/ Greenland) with values of 0.06±0.01 and 0.06±0.02, respectively. These groups also contain the lowest number of hourly means (4,7). In summer and autumn the number of allocated trajectories and hourly means drops in almost all groups due to a more instable weather situation. Remarkable for the latter two seasons is the low AOD and the marginal differences in the mean values. A clear relationship between the Ångström coefficient α and the trajectory groups can not be seen. Values of α around 1.4 are typical, indicating overall small particles. In some groups α increases with the season (from spring to autumn - 5, 7, 8) while in other groups it is nearly constant over the year (1, 2, 3, 4, 6) which indicates more homogeneous particle diameters. The largest values of the Ångström coefficient have been found for the summer value of cluster 5 as well as the fall values for clusters 7 and 8. Overall the Ångström coefficient does not depend on the time during that a trajectory was influenced by open water. Also the decrease of particle size in Ny-Ålesund in summer, which was derived from in situ measurements at the Zeppelin station Ström et al. (2003) is not as clear in our data (that contains the whole atmospheric column). This correlates only roughly with DMS production from the Arctic ocean. Hence, biogenic aerosol might be one important factor of the summer and fall aerosol but it is not the only one. Also in α the large standard deviation in spring can be seen. Hence, the aerosol over Ny-Ålesund is more variable in concentration and size in spring and more uniform during the rest of the year. Nevertheless Figure 7 displays a clear transition from the haze season to summer conditions in May when the AOD drops and the Ångström exponents increases. This transition is, however, in the column integrated optical data not so pronounced as it is in in-situ observations Tunved et al. (2012), Ström et al. (2003), which might indicate that the change in aerosol properties is more evident in the boundary layer than it is in the free troposphere.

4.2   Sodankylä

For Sodankylä 116 out of 543 trajectories had for all heights a clear affiliation to a unique cluster. Figure 4 and

Figure 5 visualize the results of the clustering for Sodankylä. The clustered trajectories and their group membership are shown in Figure 4. The allocation of τ_{500nm} and α to the trajectory groups in Figure 5 is again splitted into three seasons:

spring (red)	-	March, April, May,
summer (green)	-	June, July, August,
autumn (blue)	-	September, October, November, February.

In contrast to the results for Ny-Ålesund the group means for τ_{500nm} in Sodankylä are independent from the season and always lower than 0.08. The highest τ_{500nm} are observed for group 6 (Northern Europe/Europe), 3 (Arctic/Siberia) and 1 (Atlantic/Northern Europe) with maximum mean AOD values of 0.07±0.01 (group 6, spring), 0.07±0.03 (group 6, summer), 0.05±0.03 (group 3, spring), 0.07±0.02 (group 1, summer). It has to be remarked that the increased aerosol load in Ny-Ålesund in spring is completely absent in Sodankylä. Even though Ny-Ålesund is farther away from anthropogenic aerosol sources the springtime AOD is almost twice as high over the Spitsbergen site compared to the Fennoscandia site. Especially it is interesting to compare the clusters 3 (Arctic) and 6 (northern European) for Sodankylä. Cluster number 6 shows a slight increase in AOD (from 0.05 to 0.08) in spring and summer, this increase might be due to local pollution, while cluster number 3, at conditions which over Ny-Ålesund would have led to increased AOD, does show only clear conditions at all seasons. This means that no Arctic Haze over Sodankylä has been recorded although the right wind conditions have been present. These results compare well to a recent study from Aaltonen et al. (2012), who found that Sodankylä is generally a clear site in Finland with only a few numbers of aerosol events which occur mainly from eastern directions. This is also consistent to the work of (Stohl, 2006) who also found a mean Arctic age of air below 2 days for this site, meaning that Sodankylä is located south of the Polar-dome.

The allocated Ångström coefficients are in general higher than 1.4 in spring and summer except for group 4 (Atlantic/Canada) which shows significantly larger particles. The standard deviation of this parameter is smaller than for Spitsbergen indicating more uniform conditions with smaller particles in average for Sodankylä.

4.3   NP-35

Although there is only a short time period of measurements from NP-35 in spring 2008 available, a trajectory analysis was performed in the same way as described for Ny-Ålesund and Sodankylä. 41 out of 72 trajectories could be definitely affiliated to individual clusters. Figure 6 shows the following results:

1. high AOD especially for trajectories from the Beaufort sea (cluster 1),
2. lowest AOD for trajectories from Northeast Canada (cluster 4) and
3. in general even higher AOD than in Ny-Ålesund and Sodankylä, in March 2008.

The trajectory cluster 1 with its high AOD points to a region in North Canada for which Stohl (2006) calculated the highest Arctic age of air.

5   Linking to atmospheric circulation pattern

In the previous section we have seen that no clear connection between high AOD and air masses from inhabited regions in terms of air backtrajectories has been found. On the other hand, in Figure 7 and Figure 8 a clear seasonal dependence of not only τ_{500nm} but also α in Ny-Ålesund and Sodankylä can be seen. Moreover, both stations obviously show different seasonal cycles. For these reasons we pose in this section the question whether the Arctic AOD might be driven by atmospheric circulation pattern of scales in time and distance which are too large to be captured by air backtrajectories.

5.1   North Atlantic Oscillation (NAO)

In the following we will concentrate on Ny-Ålesund, because here we have 14 years of data and the clear annual cycle with a haze season in spring is obvious. First a simple correlation to the NAO-Index was analysed. (We used the NAO-Index from the webpage of J.Hurrell http://www.cgd.ucar.edu/cas/jhurrell/indices.html .)   The NAO-Index DJFM (December, January, February, March) describes the normed pressure ratio between the Icelandic Low and the anticyclone over the Azores. A positive NAO-Index stands for a strong pressure gradient and a meridional air mass transport from Eurasia into the Arctic. A correlation between NAO and aerosol transport into the Arctic was found by Eckhardt et al. (2003). With the help of model simulated particle transport (FLEXPART, Stohl et al. (1998)) and measured concentrations of soot and carbon monoxide they determined for Ny-Ålesund a correlation coefficient of R^2=0.41 for carbon monoxide in a positive NAO phase. However, the correlation of monthly mean τ_{500nm} and α in Figure 9 does not show any relationship between the NAO and the spring aerosol in Ny-Ålesund for our data.

This remarkable discrepancy could, among other things, be explained by the compensating effect of moisture and aerosol. If during NAO+ the increased meridional flow transports also more humidity into the Arctic, the aerosol lifetime could be reduced such that no net effect on the AOD is visible at remote sites. An accumulation of aerosol during the whole winter period as was originally suggested by Shaw (1983) would lead to a positive correlation between winter NAO-Index and spring AOD for our 14 yr data set. This idea is, however, not supported by our data. Eckhardt et al. (2003) basically considered times shorter than 30 days.

5.2   Empirical orthogonal function (EOF) analysis

The EOF analysis was applied in the following way: To quantify the connection between AOD and surface pressure pattern the principle components from the EOF DJF (December, January, February) were averaged for each year and correlated with the corresponding monthly mean τ_{500nm} in March and April. As the average of the PC gives the contribution for the corresponding EOF a possible correlation

between winter-averaged PC and spring AOD shows during which large scale circulation pattern the aerosol will occur. However, table 2 shows only low correlation coefficients with high confidence ranges. This implies again that there is no accumulation effect for τ_{500nm} detectable and that no single pressure pattern in winter is responsible for aerosol occurrence in following spring. The EOF DJF are shown in Figure 10. It can be seen that the 1.EOF DJF is similar to the NAO circulation pattern. Hence the EOF analysis and the NAO-Index correlation show the same results.

As there is no winter accumulation apparent, we further analysed a connection between the PCs of the found EOF of the monthly surface pressure and the AOD in Ny-Ålesund: The results are given in Table 3 and Figure 10. Additionally, a short time delay of up to 10 days between the EOF (surface pressure) and the AOD is considered, to account for the traveling time of air and pollutants. The largest correlations are printed bold even if they are probably not significant. March and April were chosen exemplary for the Haze season. The only noticeable correlation was found for the first two EOFs with less than 2 days time delay for March. The positive correlation coefficients indicate an airmass transport from Central Arctic and Siberia. In contrast, the negative correlation coefficients in the EOF No. 3 and 4 indicate an airmass transport from Europe, but with a time delay. This means, if there is airmass transport from Europe, the AOD can rise four or five days later. However, this correlation is hardly significant and less than for EOF No.1 and 2 (airmass transport from the Arctic and Siberia).

For the month of April the correlations are only as large as their uncertainty and in almost all EOF-AOD correlation coefficients a strong time delay can be observed. Overall the AOD at Ny-Ålesund cannot be explained well by the distribution of surface pressure. Only for March small positive correlations for air from the central Arctic (without time delay) and for Europe (with time delay) have been found. Apart from the EOFs based on surface pressure we also analysed the correlation to AOD for the pressure levels of 850, 700 and 500 hPa and found very similar results (Stock, 2010). Hence the large scale circulation alone explains only a small part of the aerosol events in Ny-Ålesund.

6   Correlation to chemical composition

The measurements at Zeppelin Mountain station above Ny-Ålesund (474 masl), contain among others, analyses of chemical trace gases and chemical speciation of particulate matter. These measurement are part of the Norwegian national monitoring programme (Aas et al., 2012) and are reported to the European Evaluation and Monitoring Programme, EMEP (Tørseth et al., 2012) and are available from http://ebas.nilu.no/. We compared these measurements with our AOD data set. First a correlation between the chemistry (daily data) and the corresponding daily mean τ_{500nm} and α is shown in Table 4. For the daily mean AOD data only measurements were used when a trajectory cluster could be assigned. In such a case in all three heights the airmasses have the same origin and the column value AOD can be compared to the chemical in-situ measurements. It can be seen that the highest correlation exists for sulphate, significant negative correlations have been

found for ammoniac and chloride ions, the latter only for the Ångström exponent.

In a second step the correlation was analysed in detail for the different trajectory clusters. For this case we only used daily means in which the trajectory cluster did not change within 24 hours, to exclude airmass changes. These results are given in Table 5. Some clear variations between the correlation of optical properties and in-situ concentration with trajectory cluster can be seen. For example, high correlations to SO_4 occur for the clusters 2, 3 and 7. Generally, the correlations for the main haze influenced clusters (1, 2) are quite different. Especially, no correlation between sulfate and AOD was found for cluster 1 (East Arctic / Siberia) which indicates that the haze clusters 1 and 2 are different in chemical composition, while similar in terms of AOD and Ångström exponent. Sea salt components (Na, Mg, Cl) do not contribute significantly to AOD according to our data. $NH4^+$ (marker for biomass burning (LeBel et al., 1991)) and $NO3^-$ (marker for anthropogenic pollution (Teinilä et al., 2003)) correlate to our measured AOD mainly for cluster 2 (Beaufort Sea) and to lesser extend for clusters 7 and 8 (local and North Atlantic).

7   Discussion

7.1   Trajectory analysis

Our data do not show a strong influence of direct transport of aerosol from inhabited regions on AOD in the Arctic. This conclusion can be drawn by two findings: 1. The AOD for the most remote site (NP-35) is highest and the AOD for the least remote site (Sodankylä) lowest. 2. The AOD in Ny-Ålesund is lower for air masses from Europe compared to air masses from the central Arctic. For this latter reasoning, however, one must consider the possibility that during direct transport from Europe into the Arctic (quick meridional transport) the air cools and clouds will form. Thus, analyzing weather-depending optical data can introduce a selection effect: the majority of direct European pollution events might have occurred under overcast conditions and have, contrary to Eckhardt et al. (2003), not been recorded here. However, our study clearly shows that air masses from Europe do not necessarily mean observation of high AOD in the Arctic. From observational point of view the possible importance of precipitation to wash out accumulation mode particles for Ny-Ålesund has been found recently by Tunved et al. (2012) using in-situ measurements. In this respect our study is in better agreement to findings from Zeppelin station. This indicates that any interpretation of aerosol events by air backtrajectories has to include precipitation properly.

The generally low AOD values over Sodankylä are remarkable. Apparently the site is quite well isolated from some important source regions as backtrajectories from central Europe or the large Russian cities are infrequent in our data. Only sporadic pollution were observed from Kola Peninsula and forest or wild fires present in northwest Russia (Aaltonen et al., 2012). Moreover, surface temperature raise well above 0°C in April already, so the air can take up more humidity and the conditions might deviate from those in the Arctic.

For Ny-Ålesund, during summer and fall mean AOD values of 0.05 (slightly decreasing with season) and Ångström exponent around 1.4 have been found. Thus, aerosol load seems to be very homogeneous in summer and fall in terms of optical properties and, therefore, principally easy to include into climate models. Only the climatologically more sensitive Haze season is heterogeneous in terms of size and number concentration. These haze events typically last for 12 hours and are related to air backtrajectories from the central Arctic, the Beaufort Sea in the North West to Siberia in the North East. Not even one aerosol event has been found for air masses from Europe (or Greenland) in our data set. The large standard deviation of the Ångstrom exponent and the AOD during spring is further analysed in Figure 11. It can be seen that no correlation exists between AOD and size of the particles. This Arctic Haze phenomenon is not discernible in our data set from Sodankylä. This station displays a constant low AOD with a little seasonal variation. (Maxima in spring and late summer and a minimum in autumn.)

7.2   Linking to atmospheric circulation

The increased AOD in Ny-Ålesund in spring can hardly be explained by the large scale circulation pattern (NAO-Index, EOF). This finding is in contrast to theories (winter accumulation by Shaw (1983)) and other observations (carbon monoxide by Eckhardt et al. (2003)). However, contrary to trace gases aerosol can react and be modified between emission and its arrival in the Arctic, namely by gas to particle conversion (new particle formation) and aerosol cloud interactions (rain out, wash out). For this reason it is not surprising that the effective pollution pathways into the Arctic might be different for trace gases and chemically inert, water insoluble aerosol on the one hand and (the majority) of hygroscopic aerosol on the other hand.

Knowledge of detailed weather information in the central Arctic, including moisture and precipitation is, hence, urgently required for a better understanding of aerosol occurrences. In April, although still a month of the haze season in Ny-Ålesund, the correlation to EOFs drops further to the level of insignificance. At the same time sunlight increases which might accelerate as well photochemistry as wet scavenging.

7.3   Correlation to chemical composition

The positive correlation between τ_{500nm} and SO_4^{2-} in Table 4 implies firstly, that the higher the AOD the higher the sulfate concentration in the atmosphere and secondly, that most of the optical active particles in our data set contain sulfate. This is in agreement to numerous studies, for example a chemical analysis of Hara et al. (2003), even if their results were obtained for one of the few direct transport events of Arctic haze in spring 2000 or Teinilä et al. (2003) and references therein. Therefore we are confident that our AOD data set represents the typical aerosol events indeed. Overall, sea salt does not represent an important aerosol constituent in our data set. The anti-correlation between CL^- and the Ångström exponent means that large particles contain more fresh sea salt, but their contribution to the AOD is negligible. Sea salt aerosol has been found in

the boundary layer of Ny-Ålesund (Weinbruch et al., 2012) but is according to our data not important for the atmospheric column.

From this chemical analysis one can see a clear difference between the haze clusters 1 (East Arctic / Siberia) and 2 (Beaufort sea). Cluster 2 correlates well to the anthropogenic markers (SO_4^{2-}, NH_4^+ and NO_3^-), but based on the air trajectories the source region might be located in East Asia, not in Europe (including European Russia). Cluster 1, however, must be more diverse chemically as neither anthropogenic, nor soil (K^+, Mg^+, Ca^{2+}) nor sea salt components alone correlate to the AOD.

NH_3 is the most important base that neutralizes H_2SO_4 (Whitlow et al., 1994; Kühnel et al., 2011). Hence, it disappears quickly in acidic air and the anti-correlation between ammonia and AOD means that the aerosol tends to arrive in more acid conditions. However, our NH_3 measurements are more uncertain than the other components due to problems with contamination of filters (Aas et al., 2012) and the fact that the filter-pack method is biased when it comes to separating gaseous NH_4^+ and particulate NH_4^+ (EMEP, 1996). Nevertheless an anti-correlation between NH_3 and AOD can be seen which is mainly found for the clusters 5 (Europe), 6 (Central Arctic) and 7 (Local Arctic), but only weak for the high AOD clusters 1 (East Arctic) and 2 (Beaufort Sea). Overall the correlation between AOD and chemical composition varies between the clusters.

8   Conclusion

The main conclusions of this work are:

The correlation between AOD and 5-day backtrajectories does not show a clear origin of the aerosol. This means that the lifetime of aerosol is longer and/or the aerosol is modified in the Arctic and appears in air masses which, due to the growing insecurity of air backtrajectory calculation at remote places, have unknown origin.

The correlation between the AOD and the general circulation pattern is only weak. A dependence on the NAO phase has not be seen. In this respect aerosol and trace gases seem to be different. A facilitated meridional transport into the Arctic (NAO+) does not increase the AOD over Ny-Ålesund.

Direct transport of air masses from Europe do not necessarily mean increased AOD as if the European sources were not essential. From the difference between our finding and previous work (among others Eneroth et al. (2003)) we hypothesize that direct transport of polluted air masses from Europe into the Arctic very frequently goes ahead with cloud formation - and these cases cannot be seen with our photometers. Moreover we hypothesize that increased meridional transport during NAO+ carries not only aerosol/precursor gases but also humidity into the Arctic and that apparently increased wet scavenging occurs which in turn washes out the originally higher aerosol load.

We found remarkable low AOD for Sodankylä without any haze event.

We found higher AOD for Ny-Ålesund for air currents from the Eastern or central Arctic.

From the comparison of clusters and sites with high or low AOD one gets the impression that the AOD might better

be correlated with low temperatures of the air along their path. This is an open task for future work.

The AOD over Ny-Ålesund does correlate strongly with sulfate. Chemically, only the haze from cluster 2 (Beaufort Sea) contains anthropogenic markers. The high AOD cases from clusters 1 (East Arctic / Siberia) and 6 (Central Arctic) are chemically more diverse.

As the origin of the optically detectable aerosol could not be found in a satisfying way in this work, two strategies for further investigations are proposed:

Coordinated observations of aerosol/AOD at different Arctic sites should be performed to determine the spatial and temporal extend of aerosol events and see whether there is a common Arctic reservoir for aerosol or precursors. Especially measurements in Siberia or above the Arctic ocean are highly needed as these sites are closer to the sources of aerosol seen in Ny-Ålesund.

Aircraft campaigns for aerosol and cloud measurements which follow pollution plumes into the Arctic at least for several days are proposed to really monitor the pollution pathways and the possible role of cloud formation and aerosol alteration.

REFERENCES

V. Aaltonen, E. Rodriguez, S. Kazadzis, A. Arola, V. Amiridis, H. Lihavainen, and G. de Leeuw. On the variation of aerosol properties over Finland based on the optical columnar measurements. *Atm. Res.*, 116:46–55, 2012. 10.1016/j.atmosres.2011.07.014.

W. Aas, S. Solberg, S. Manø, and K.E. Yttri. Monitoring of long-range transported air pollutants. Annual report 2011. Technical Report Norwegian Klif report 126/2012. NILU OR 19/2012, Norwegian Institute for Air Research, Kjeller, 2012.

T.N. Carlson. Speculations on the movement of polluted air to the Arctic. *Atmosph. Environ.*, 15:1473–1477, 1981. 10.1016/0004-6981(81)90354-1.

D. Dommenget and M. Latif. A Cautionary Note on the Interpretation of EOFs. *Journal of Climate*, 15:216–225, 2002.

S.R. Dorling, T.D. Davies, and C.E. Pierce. Cluster analysis: A technique for estimating the synoptic meteorological controls on air and precipitation chemistry - method and applications. *Atm. Env.*, 26A(14):2575–2581, 1992.

S. Eckhardt, A. Stohl, S. Beirle, N. Spichtinger, P. James, C. Forster, C. Junker, T. Wagner, U. Platt, and S.G. Jennings. The North Atlantic Oscillation controls air pollution transport to the Arctic. *Atmos. Chem. Phys.*, 3:1769–1778, 2003.

EMEP. *EMEP manual for sampling and chemical analysis.* NILU - Norwegian Institute for Air Research, N-2007 Kjeller, Norway, ccc-report 1/95 edition, 1996. Revision 2001.

K. Eneroth, E. Kjellström, and K. Holmén. A trajectory climatology for Svalbard; investigating how atmospheric flow patterns

influence observed tracer concentrations. *Physics and Chemsitry of the Earth*, 28:1191–1203, 2003. `10.1016/j.pce.2003.08.051`.

J. A. Fisher, D. J. Jacob, M. T. Purdy, M. Kopacz, P. Le Sager, C. Carouge, C. D. Holmes, R. M. Yantosca, R. L. Batchelor, K. Strong, G. S. Diskin, H. E. Fuelberg, J.S. Holloway, E. J. Hyer, W. W. McMillan, J. Warner, D. G. Streets, Q. Zhang, Y. Wang, and S. Wu. Source attribution and interannual variability of Arctic pollution in spring constrained by aircraft (ARCTAS, ARCPAC) and satellite (AIRS) observations of carbon monoxide. *Atmos. Chem. Phys.*, 10:977–996, 2010. `10.5194/acp-10-977-2010`.

J.K. Gibson, P. Kallberg, S. Uppala, A. Hernandez, A. Nomura, and E. Serrano. ECMWF Re-Analysis Project Report Series, 1.ERA-15 Description. Technical report, European Centre for Medium-Range Weather Forecasts, 1999.

A. Hall and X. Qu. Using the current seasonal cycle to constrain snow albedo feedback in future climate change. *Geophys. Res. Lett.*, 33:L03502, 2006. `10.1029/2005GL025127`.

A. Hannachi, I. T. Jolliffe, and D. B. Stephenson. Empirical orthogonal functions and related techniques in atmospheric sciences: a review. *International Journal of Climatology*, 27: 1119 –1152, 2007. `10.1002/joc.1499`.

K. Hara, S. Yamagata, T. Yamanouchi, K. Sato, A. Herber, Y. Iwasaka, M. Nagatani, and H. Nakata. Mixing states of individual aerosol particles in spring Arctic troposphere during ASTAR 2000 campaign. *Journal of Geophys. Res.*, 108 (D7), 2003. `10.1029/2002JD002513`.

A. Herber, L.W. Thomason, H. Gernandt, U. Leiterer, D. Nagel, K.-H. Schulz, J. Kaptur, T. Albrecht, and J. Notholt. Continuous day and night aerosol optical depth observations in the Arctic between 1991 and 1999. *Journal of Geophys. Res.*, 107 (D10), 2002. `10.1029/2001JD000536`.

A. Hoffmann, C. Ritter, M. Stock, M. Maturilli, and R. Neuber. Lidar measurements of the Kasatochi aerosol plume in August and September 2008 in Ny-Ålesund, Spitsbergen. *Journal of Geophys. Res.*, 2010.

T. Iversen. On the atmospheric transport of pollution to the Arctic. *Geophys. Res. Lett.*, 11:457–460, 1984. `10.1029/GL011i005p00457`.

R. Jaiser, K. Dethloff, D. Handorf, A. Rinke, and J. Cohen. Impact of sea ice cover changes on the Northern Hemisphere atmospheric winter circulation. *Tellus A*, 64:11595, 2012. `10.3402/tellusa.v64i0.11595`.

R. Kühnel, T.J. Roberts, M.P. Björkman, E.Isaksson, W. Aas, K. Holmén, and J. Ström. 20-Year Climatology of NO3- and NH4+ Wet Deposition at Ny-Ålesund, Svalbard. *Advances in Meteorology*, 2011, 2011. `10.1155/2011/406508`. Article ID 406508, 10 pages.

P.J. LeBel, S.A. Vay, and P.D. Roberts. Ammonia and nitric acid emissions from wetlands and boreal forest fires. *Global biomass burning (ed. J.S. Levine) Cambridge, Mass. MIT Press*, pages 225–229, 1991.

J. MacQueen. Some methods for classification and analysis of multivariate observations. In L.M. Le Cam and J. Neyman, editors, *Proceedings of the Fifth Berkeley Symposium an Mathematical Statistics and Probability*, pages 281 – 297. Univ. California Press, Berkeley, 1967.

M. Mazzola, R.S. Stone, A. Herber, C. Tomasi, A. Lupi, V. Vitale, C. Lanconelli, C. Toledano, V.E. Cachorro, N.T. O'Neill, M. Shiobara, V. Aaltonen, K. Stebel, T. Zielinski, T. Petelski, J.P. Ortiz de Galisteo, B. Torres, A. Berjon, P. Goloub, Z. Li, L. Blarel, I. Abboud, E. Cuevas, M. Stock, K.-H. Schulz, and A. Virkkula. Evaluation of sun photometer capabilities for retrievals of aerosol optical depth at high latitudes: The POLAR-AOD intercomparison campaigns. *Atm. Env.*, 52:4–17, 2012. `10.1016/j.atmosenv.2011.07.042`.

N.T. O'Neill. Properties of Sarychev sulphate aerosols over the Arctic. *J. Geophys. Res.*, 117:D04203, 2012. `10.1029/2011JD016838`.

T. Orgis, S. Brand, U. Schwarz, D. Handorf, K. Dethloff, and J. Kurths. Influence of interactive stratospheric chemistry on large-scale air mass exchange in a global circulation model. *European Physical Journal Special Topics*, 174, 2009.

R. Preisendorfer. *Principal Component Analysis in Meteorology and Oceanography*, volume 17. Elsevier, 1988.

P.K. Quinn, G. Shaw, E. Andrews, E.G. Dutton, T. Ruoho-Airola, and S.L. Gong. Arctic haze: current trends and knowledge gaps. *Tellus B*, 59:99–114, 2007. `10.1111/j.1600-0889.2006.00238.x`.

A. Rozwadowska, T. Zielinski, T. Petelski, and P. Sobolewski. Cluster analysis of the impact of air back-trajectories on aerosol optical properties at Hornsund, Spitsbergen. *Atmos. Chem. Phys.*, 10:877–893, 2010.

J.A. Screen and I. Simmonds. The central role of diminishing sea ice in recent Arctic temperature amplification. *Nature*, 464: 1334–1337, 2010. `10.1038/nature09051`.

G.E. Shaw. Evidence for a central Eurasian source area of Arctic haze in Alaska. *Nature*, 299:815–818, 1983.

G.E. Shaw. The Arctic Haze Phenomenon. *Bull. Amer. Meteo. Soc.*, 76:2403–2413, 1995.

S. Solomon, D. Qin, M. Manning, Z. Chen, M. Marquis, K.B. Averyt, M. Tignor, and H.L. Miller. *Climate Change 2007: The Physical Science Basis*. Cambridge University Press, Cambridge, United Kingdom and New York, NY, USA, 2007.

M. Stock. *Charakterisierung der troposphärischen Aerosolvariabilität in der europäischen Arktis*. PhD thesis, University Potsdam, 2010. URL `URL:http://opus.kobv.de/ubp/volltexte/2010/4920`.

M. Stock, C. Ritter, A. Herber, W. von Hoyningen-Huene, K. Baibakov, J. Grser, T. Orgis, R. Treffeisen, N. Zinoviev, A. Makshtas, and K. Dethloff. Springtime Arctic aerosol: Smoke versus Haze, a case study for March 2008. *Atm. Env.*, 52:48–55, 2011. `10.1016/j.atmosenv.2011.06.051`.

A. Stohl. Characteristics of atmospheric transport into the Arctic troposphere. *Journal of Geophys. Res.*, 111, 2006. `10.1029/2005JD006888`.

A. Stohl, M. Hittenberger, and G. Wotawa. Validation of the Lagrangian particle dispersion model FLEXPART against large scale tracer experiments. *Atmospheric Environment*, 32:4245–4264, 1998.

A. Stohl, E. Andrews, J.F. Burkhart, C. Forster, A. Herber, S.W. Hoch, D. Kowal, C. Lunder, T. Mefford, J.A. Ogren, S. Sharma, N. Spichtinger, K. Stebel, R. Stone, J. Str"øm, K. Tørseth, C. Wehrli, and K.E. Yttri. Pan-Arctic enhancements of light absorbing aerosol concentrations due to North American boreal forest fires during summer 2004. *Journal of Geophys. Res.*, 111, 2006. `10.1029/2006JD007216`.

A. Stohl, T. Berg, J.F. Burkhart, A.M. Fjæraa, C. Forster, A. Herber, Ø. Hov, C. Lunder, W.W. McMillan, S. Oltmans, M. Shiobara, D. Simpson, S. Solberg, K. Stebel, J. Ström, K. Tørseth, R. Treffeisen, K. Virkkunen, and K.E. Yttri. Arctic smoke - record high air pollution levels in the European Arctic due to agricultural fires in Eastern Europe in Spring 2006. *Atmospheric Chemistry and Physics*, 7:511–534, 2007.

R. S. Stone, G .P Anderson, S. Sharma, A. Herber, E. G. Dutton, K. Eleftheriadis, S-M Li, A. Jefferson, and D. Nelson. A characterization of Arctic aerosols and their radiative impact on the surface radiation budget. *International Journal of Climatology*, 2013. submitted.

J.C. Stroeve, M.C. Serreze, M.M. Holland, J.E. Kay, J. Malanik, and A.P. Barrett. The Arctics rapidly shrinking sea ice cover: a research synthesis. *Climatic Change*, 110:1005–1027, 2012. `10.1007/s10584-011-0101-1`.

J. Ström, J. Umegård, K. Tørseth, P. Tunved, H.-C. Hansson, K. Holmén, V. Wismann, A. Herber, and G. König-Langlo.

One year of particle size distribution and aerosol chemical composition measurements at the Zeppelin Station, Svalbard, March 2000March 2001. *Phys. and Chem. of the Earth*, 28: 1181–1190, 2003.

B.J. Stunder. An assessment of the quality of forecast trajectories. *Journal of Appl. Meteo.*, 35:1319–1331, 1996.

K. Teinilä, R. Hillamo, and V.-M. Kerminen H.J. Beine. Aerosol chemistry during the NICE dark and light campaigns. *Atm. Env.*, 37:563–575, 2003.

C. Toledano, V.E. Cachorro, M. Gausa, K. Stebel, V. Aaltonen, A. Berjón, J.P. Ortiz de Galisteo, A.M. de Frutos, Y. Bennouna, S. Blindheim, C.L. Myhre G. Zibordi, C. Wehrli, S. Kratzerg, B. Hakansson, T. Carlund, G. de Leeuw, A. Herber, and B. Torres. Overview of sun photometer measurements of aerosol properties in Scandinavia and Svalbard. *Atm. Env.*, 52:18–28, 2012. `10.1016/j.atmosenv.2011.10.022`.

K. Tørseth, W. Aas, K. Breivik, A.M. Fjæraa, M. Fiebig, A.G. Hjellbrekke, C. Lund Myhre, S. Solberg, and K.E. Yttri. Introduction to the European Monitoring and Evaluation Programme (EMEP) and observed atmospheric composition change during 19722009. *Atmos. Chem. Phys.*, 12:5447–5481, 2012. `10.5194/acp-12-5447-2012`.

P. Tunved, J. Ström, and R. Krejci. Arctic aerosol life cycle: linking aerosol size distributions observed between 2000 and 2010 with air mass transport and precipitation at Zeppelin station, Ny-lesund, Svalbard. *Atmos. Chem. Phys. Discuss.*, 12:29967–30019, 2012. `doi:10.5194/acpd-12-29967-2012`.

S. M. Uppala, P. W. Kållberg, A.J. Simmons, U. Andrae, V. Bechtold, M. Fiorino, and coauthors. The ERA-40 reanalysis. *Quarterly Journal of the Royal Meteorological Society*, 131: 2961–3012, 2005. `0.1256/qj.04.176`.

H. von Storch and F.W. Zwiers. *Statistical Analysis in Climate Research*. Cambridge University Press, 2001.

C. Warneke, R. Bahreini, J. Brioude, C.A. Brock, J.A. de Gouw, D.W. Fahey, K.D. Froyd, J.S. Holloway, A. Middlebrook, L. Miller, S. Montzka, D.M. Murphy, J. Peischl, T.B. Ryerson, J.P. Schwarz, J.R. Spackman, and P. Veres. Biomass burning in Siberia and Kazakhstan as an important source for haze over Alaskan Arctic in April 2008. *Geophys. Res. Letters*, 36, 2009. `10.1029/2008GL036194`.

S. Weinbruch, D. Wiesemann, M. Ebert, K. Schütze, R. Kallenborn, and J.Ström. Chemical composition and sources of aerosol particles at Zeppelin Mountain (Ny Ålesund, Svalbard): An electron microscopy study. *Atm. Env.*, 49:142–150, 2012. `10.1016/j.atmosenv.2011.12.008`.

S. Whitlow, P. Mayewski, J. Dibb, G. Holdsworth, and M. Twickler. An ice-core based record of biomass burning in the Arctic and Subarctic, 1750 – 1980. *Tellus B*, 46 (3):234–242, 1994.

WMO. Guide to Meteorological Instruments an Methods of Observation. *World Meteorological Organisation, Geneva*, WMO-No.8, 1996.

T. Yamanouchi, R. Treffeisen, A. Herber, M. Shiobara, S. Yamagata, K. Hara, K. Sato, M. Yabuki, Y. Tomikawa, A. Rinke, R. Neuber, R. Schumachter, M. Kriews, J. Ström, O. Schrems, and H. Gernandt. Arctic Study of Tropospheric Aerosol and Radiation (ASTAR) 2000: Arctic haze case study. *Tellus*, 57B: 141–152, 2005.
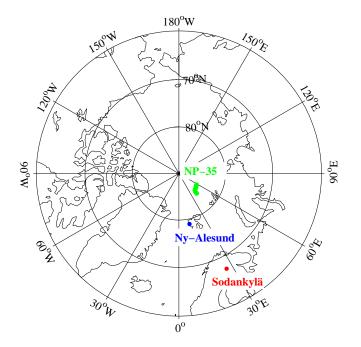
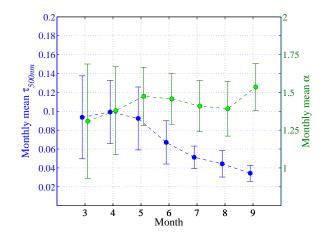**Figure 1.** Position of Ny-Ålesund, Sodankylä and NP-35 in March/April 2008.

Figure 7. Monthly means of τ_{500nm} and α in Ny-Ålesund.

Table 1. Number and wavelength range of the interference filters in the sun photometer types SP2H, SP1A and PFR.

Type	SP2H	SP1A	PFR
channels	14	17	4
wavelengths	360–1050nm	350–1090nm	368–862nm

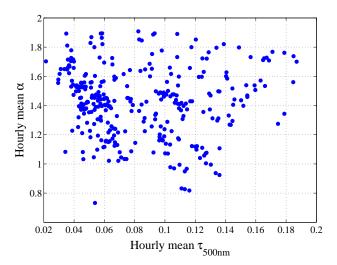**Figure 8.** Monthly means of τ_{500nm} and α in Sodankylä.

Figure 11. Scatter plot of all hourly mean τ_{500nm} and α measured in Ny-Ålesund 1995–2008 and assigned to a trajectory cluster.
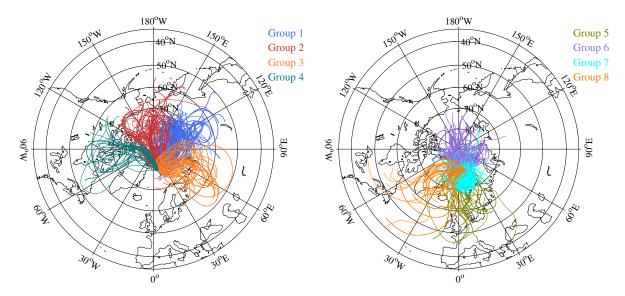
Figure 2. Cluster allocation of ensemble trajectories at all heights (850, 700 and 500 hPa) for Ny-Ålesund 1995–2008.
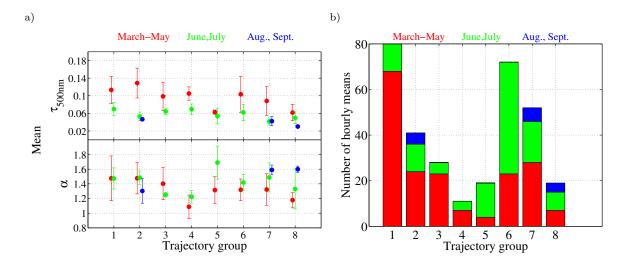

Figure 3. a) Mean values and standard deviation of τ_{500nm} and α and b) number of hourly mean AOD in different trajectory groups from Ny-Ålesund 1995–2008. Seasonally separation: spring – red, summer – green, autumn – blue.

Table 2. Correlation coefficients and confidence range for the correlation between the principle components (PC) of the first five EOF MSLP DJF and the monthly mean τ_{500nm} of March and April in Ny-Ålesund (1995–2008).

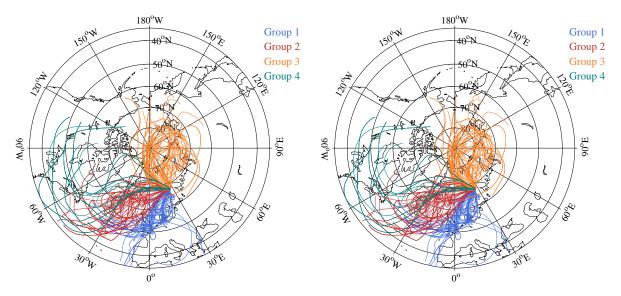| Month	R				
	1.EOF	2.EOF	3.EOF	4.EOF	5.EOF
March	-0.08±0.56	-0.16±0.55	-0.12±0.56	-0.27±0.53	-0.14±0.55
April	-0.08±0.59	-0.19±0.57	-0.05±0.59	-0.04±0.59	0.15±0.58

Figure 4. Cluster allocation of ensemble trajectories at all heights (850, 700 and 500 hPa) for Sodankylä 2004–2007.
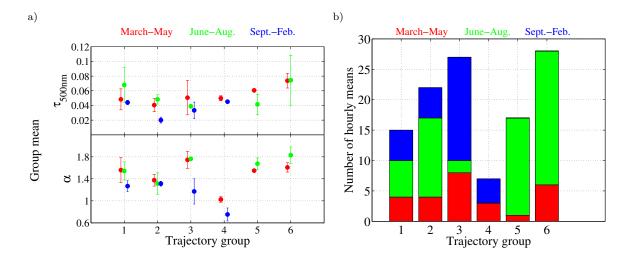

Figure 5. a) Mean values and standard deviation of τ_{500nm} and α and b) number of hourly mean AOD in different trajectory groups from Sodankylä 2004–2007. Seasonally separation: spring – red, summer – green, autumn – blue.

Table 3. Correlation coefficients and confidence range for the correlation between the principle components (PC) of the first five EOF MSLP March and April and the daily mean τ_{500nm} of March and April in Ny-Ålesund (1995–2008).

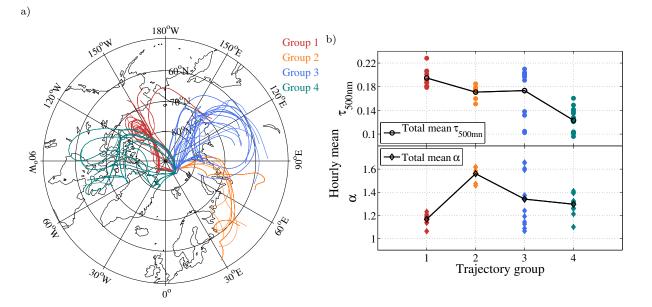|	March R					April R				
	1.EOF	2.EOF	3.EOF	4.EOF	5.EOF	1.EOF	2.EOF	3.EOF	4.EOF	5.EOF
0	**0.41 ±0.22**	**0.36 ±0.29**	0.05 ±0.26	0.02 ±0.26	-0.11 ±0.26	-0.03 ±0.20	0.0 ±0.20	0.17 ±0.19	0.17 ±0.19	-0.02 ±0.20
1	0.37 ±0.22	0.32 ±0.23	0.03 ±0.26	0.08 ±0.26	-0.10 ±0.26	-0.03 ±0.20	0.02 ±0.20	**0.19 ±0.19**	0.15 ±0.19	0.02 ±0.20
2	0.27 ±0.24	0.30 ±0.23	-0.05 ±0.26	0.06 ±0.26	-0.10 ±0.25	-0.03 ±0.20	0.03 ±0.20	**0.19 ±0.19**	0.15 ±0.19	0.05 ±0.20
3	0.19 ±0.25	0.32 ±0.23	-0.16 ±0.25	-0.03 ±0.25	-0.05 ±0.25	-0.05 ±0.20	0.07 ±0.20	**0.19 ±0.19**	0.14 ±0.19	0.04 ±0.20
4	0.13 ±0.24	0.34 ±0.22	**-0.24 ±0.23**	-0.13 ±0.24	0.04 ±0.25	-0.10 ±0.19	0.14 ±0.19	0.16 ±0.19	0.09 ±0.20	0.01 ±0.20
5	0.11 ±0.24	0.32 ±0.22	-0.23 ±0.23	**-0.20 ±0.24**	0.13 ±0.24	-0.10 ±0.20	0.20 ±0.19	0.16 ±0.19	-0.04 ±0.20	-0.05 ±0.20
6	0.12 ±0.24	0.29 ±0.22	-0.16 ±0.23	-0.18 ±0.23	0.20 ±0.23	-0.04 ±0.20	0.25 ±0.18	0.11 ±0.19	-0.16 ±0.19	-0.08 ±0.20
7	0.11 ±0.23	0.25 ±0.22	-0.10 ±0.23	-0.08 ±0.23	**0.25 ±0.22**	-0.01 ±0.20	**0.26 ±0.18**	0.02 ±0.20	**-0.23 ±0.19**	-0.09 ±0.20
8	0.10 ±0.23	0.17 ±0.22	-0.06 ±0.23	0.02 ±0.23	0.22 ±0.22	0.07 ±0.20	0.19 ±0.19	-0.02 ±0.20	**-0.23 ±0.19**	-0.10 ±0.20
9	0.11 ±0.22	0.12 ±0.22	-0.04 ±0.22	0.07 ±0.22	0.11 ±0.22	0.15 ±0.19	0.15 ±0.19	-0.06 ±0.20	-0.19 ±0.19	**-0.11 ±0.19**
10	0.12 ±0.22	0.10 ±0.22	-0.02 ±0.22	0.09 ±0.22	0.05 ±0.22	**0.17 ±0.19**	0.18 ±0.19	-0.11 ±0.19	-0.15 ±0.19	-0.05 ±0.20

a)

Figure 6. a) Clustering of the ensemble trajectories at all heights (850, 700, 500 hPa) from NP-35 between 14 March and 7 April, 2008, and b) hourly mean of τ_{500nm} and α in the different trajectory groups and the group mean of τ_{500nm} and α.
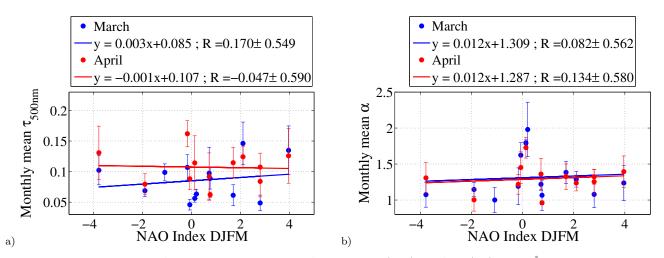

Figure 9. Correlation between NAO-Index and monthly mean AOD in March (blue) and April (red) for Ny-Ålesund 1995–2008. Drawn are the monthly mean standard deviation and the linear regression of a) τ_{500nm} and b) α. The parameters of the regression, including the correlation coefficient and their confidence range, are shown in the legend.

Table 4. Correlation coefficients and confidence range between the measured τ_{500nm} / α in Ny-Ålesund, which were assigned a trajectory cluster, and the measured concentration of different atmospheric chemical components at Zeppelin. (g = gas, s = solid).

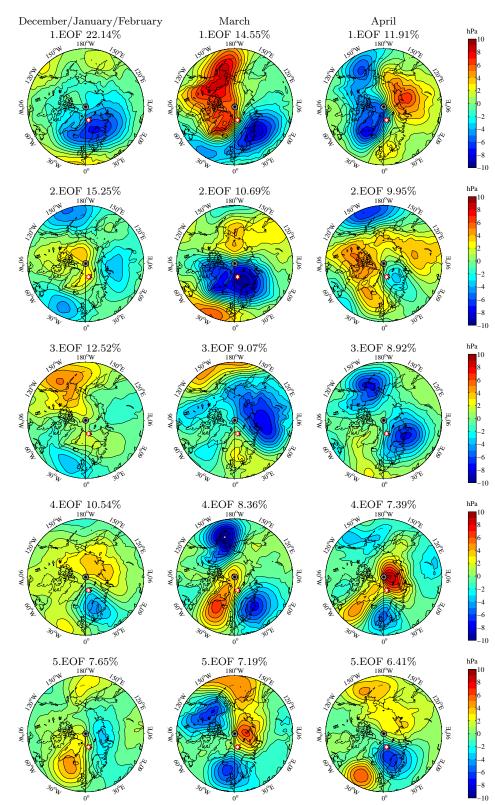| Matter	$R(\tau_{500nm})$	$R(\alpha)$	Number of daily means	Period
SO_4^{2-}(s)	**0.506 $\pm$0.144**	0.124 $\pm$0.191	103	
NO_3^-(s)	0.070 $\pm$0.193	0.160 $\pm$0.189	103	
NH_4^+(s)	0.185 $\pm$0.186	0.148 $\pm$0.188	105	
Na^+(s)	0.028 $\pm$0.192	-0.055 $\pm$0.192	105	
Mg^{2+}(s)	-0.014 $\pm$0.192	-0.238 $\pm$0.181	105	
Ca^{2+}(s)	-0.020 $\pm$0.192	-0.075 $\pm$0.191	105	1995 - 2008
K^+(s)	-0.051 $\pm$0.192	-0.019 $\pm$0.192	105	
Cl^-(s)	0.123 $\pm$0.191	**-0.272 $\pm$0.180**	103	
SO_2(g)	0.052 $\pm$0.192	-0.024 $\pm$0.192	105	
NH_3(g)	**-0.259 $\pm$0.179**	0.202 $\pm$0.184	105	

Figure 10. First five EOF of mean sea level pressure of three periods: left-December, January and February (1995–2008), middle-March (1995–2008), right-April(1995–2008) and their variance in %. The white star marks the position of Ny-Ålesund, respectively Spitsbergen.

Table 5. Correlation coefficients and confidence range between the measured τ_{500nm} in Ny-Ålesund, which were assigned to a unique trajectory cluster, and the measured concentration of different atmospheric chemical components at Zeppelin. (g = gas, s = solid).

Matter	$R(\tau_{500nm})$							
	1	2	3	4	5	6	7	8
SO_4^{2-}(s)	$0.174_{\pm0.436}$	$\mathbf{0.765_{\pm0.218}}$	$\mathbf{0.761_{\pm0.291}}$	$0.180_{\pm1.095}$	$0.421_{\pm0.570}$	$0.379_{\pm0.407}$	$\mathbf{0.573_{\pm0.329}}$	$0.460_{\pm0.631}$
NO_3^-(s)	$0.040_{\pm0.449}$	$\mathbf{0.567_{\pm0.355}}$	$0.013_{\pm0.693}$	$-0.154_{\pm1.105}$	$-0.345_{\pm0.611}$	$0.161_{\pm0.463}$	$-0.005_{\pm0.490}$	$0.049_{\pm0.798}$
NH_4^+(s)	$0.049_{\pm0.449}$	$\mathbf{0.743_{\pm0.235}}$	$0.311_{\pm0.626}$	$0.382_{\pm0.837}$	$0.237_{\pm0.654}$	$-0.008_{\pm0.475}$	$\mathbf{0.694_{\pm0.254}}$	$\mathbf{0.601_{\pm0.511}}$
Na^+(s)	$-0.076_{\pm0.447}$	$0.035_{\pm0.523}$	$0.104_{\pm0.686}$	$0.016_{\pm0.980}$	$-0.367_{\pm0.600}$	$-0.373_{\pm0.409}$	$0.264_{\pm0.456}$	$-0.227_{\pm0.759}$
Mg^{2+}(s)	$-0.187_{\pm0.434}$	$-0.088_{\pm0.520}$	$0.134_{\pm0.681}$	$-0.165_{\pm0.953}$	$-0.167_{\pm0.674}$	$-0.213_{\pm0.454}$	$0.422_{\pm0.403}$	$0.050_{\pm0.798}$
Ca^{2+}(s)	$-0.139_{\pm0.441}$	$0.096_{\pm0.519}$	$-0.047_{\pm0.691}$	$-0.263_{\pm0.912}$	$0.021_{\pm0.693}$	$0.053_{\pm0.474}$	$0.110_{\pm0.484}$	$0.014_{\pm0.800}$
K^+(s)	$0.045_{\pm0.449}$	$-0.179_{\pm0.507}$	$0.265_{\pm0.644}$	$-0.033_{\pm0.979}$	$-0.391_{\pm0.587}$	$-0.220_{\pm0.452}$	$0.073_{\pm0.487}$	$\mathbf{-0.726_{\pm0.378}}$
Cl^-(s)	$-0.068_{\pm0.448}$	$-0.035_{\pm0.523}$	$0.020_{\pm0.693}$	$0.171_{\pm1.099}$	$-0.194_{\pm0.667}$	$0.060_{\pm0.474}$	$0.300_{\pm0.446}$	$0.033_{\pm0.799}$
SO_2(g)	$0.201_{\pm0.432}$	$-0.149_{\pm0.512}$	$0.002_{\pm0.693}$	$0.116_{\pm0.967}$	$0.066_{\pm0.690}$	$-0.103_{\pm0.470}$	$-0.166_{\pm0.477}$	$0.139_{\pm0.785}$
NH_3(g)	$-0.049_{\pm0.449}$	$-0.224_{\pm0.498}$	$-0.197_{\pm0.666}$	$-0.054_{\pm0.977}$	$-0.471_{\pm0.539}$	$\mathbf{-0.462_{\pm0.374}}$	$\mathbf{-0.492_{\pm0.372}}$	$-0.285_{\pm0.735}$
number of daily means	20	15	9	5	9	18	17	7